A MONTE CARLO CORRECTION FOR THE EFFECT OF COMPTON SCATTERING IN 3-D PET BRAIN IMAGING

C.S. Levin, M. Dahlbom, E.J. Hoffman
UCLA School of Medicine Division of Nuclear Medicine and Biophysics
Los Angeles, CA 90024

Abstract

A Monte Carlo simulation has been developed to simulate and correct for the effect of Compton scatter in 3-D acquired PET brain scans. The method utilizes the 3-D reconstructed image volume as the source intensity distribution for a photon-tracking Monte Carlo simulation. It is assumed that the number of events in each pixel of the image represents the isotope concentration at that location in the brain. The history of each annihilation photon's interactions in the scattering medium is followed, and the sinograms for the scattered and unscattered photon pairs are generated in a simulated 3-D PET acquisition. The calculated scatter contribution is used to correct the original data set. The method is general and can be applied to any scanner configuration or geometry. In its current form the simulation requires 25 hours on a single Sparc10 CPU when every pixel in a 15-plane, 128x128 pixel image volume is sampled, and less than 2 hours when 16 pixels (4x4) are grouped as a single pixel. Results of the correction applied to 3-D human and phantom studies are presented.

I. INTRODUCTION

In order for PET to realize its full potential in terms of spatial resolution and signal-to-noise ratio [1], many systems are now designed with retractable inter-plane septa, allowing all possible lines of response to be acquired [2, 3]. Unfortunately, this three-dimensional (3-D) mode of acquisition results in a large (ca. 3-fold) increase in scatter fraction relative to conventional two-dimensional data collections with septa. This increase in scatter compromises accuracy in quantitation and degrades image contrast. The development of an accurate and efficient scatter correction is desirable for the removal of image distortions which might lead to diagnostic errors, and essential before quantitative measurements can be made with 3-D PET.

Currently, a number of approaches to scatter correction for 3-D PET [3-10] are described in the literature. Most of these methods use models of scatter that are presumed to be valid without regard to the source distribution and attenuating media. Scatter distributions for realistic sources and scattering media do have a significant dependence on the source distribution and object composition and shape. Most generalizations or simplifying assumptions should not be expected to hold for all situations and will compromise accuracy. In addition, methods that require supplementary measurements introduce additional noise and may require longer patient scanning time and/or larger data sets.

The dual energy method [4] assumes the spatial distribution of scattered events present in photo-peak window data is essentially the same as that in a second, lower energy window. The method also doubles an already large 3-D data set. The Convolution/subtraction approach [3, 5, 6] assumes that the Compton scatter distribution is an empirically determined integral transformation of the 3-D emission data. This scatter kernel is usually derived from phantom measurements, assuming that one size and shape is adequate. The 2-D/3-D difference method [7] relies on the smoothness of the scatter distribution and uses an additional 2-D scan to estimate scatter in the oblique planes using the direct plane data. The interpolation fitting technique [8] assumes the scatter distribution is a certain shape function, which can be fitted to the tails of profiles outside the object. The success of the fits depends on the symmetry of the activity distributions and on the presence of tails with adequate statistics. Analytic techniques [9,10] directly calculate the scatter using the emission and/or transmission data. These methods utilize various approximations, such as, assuming only one photon scatters per annihilation pair, to reduce computation time.

As a preliminary effort to correct for Compton scatter in 3-D whole-body PET imaging, a Monte Carlo simulation has been developed to simulate and correct for scatter in 3-D PET brain imaging [11]. This method models the statistical and physical process of photon emission and simulates the scatter distribution for complex activity and density distributions using only the 3-D reconstructed image volume, the detector gantry geometry and the physics of photon interactions. No assumptions are made of the shapes of the source distributions or attenuation media. However, the large computational burden may necessitate the use of faster hardware or parallel computing to make this approach feasible for routine clinical use. Execution time can also be reduced by using suitable coarse sampling of the input image with little loss in accuracy. The goal of this paper is to demonstrate the ability of the Monte Carlo simulation to accurately model and correct for Compton scatter in complex 3-D activity distributions and attenuating media.

II. METHODS

The Monte Carlo scatter correction is isotope distribution dependent, and requires the 3-D reconstructed image volume as input. Corrections for normalization and attenuation are assumed to be accurate. The concept for the program input is depicted in Figure 1. The input image volume is treated as a three-dimensional source intensity distribution for a photon-tracking simulation; it is assumed that the number of counts in each pixel of the image represents the isotope concentration at that location. The image volume planes are stacked and placed in the simulated scanner, assuming a common axis. The geometry of the detector gantry is determined by the number and size of individual detector crystals per ring, including spaces. The program then follows the history of each photon and its interactions in the scatter medium and traces escaping photons into the detector gantry in a simulated 3-D PET acquisition. The distributions of the unscattered (pri-

0018-9499/95$4.00

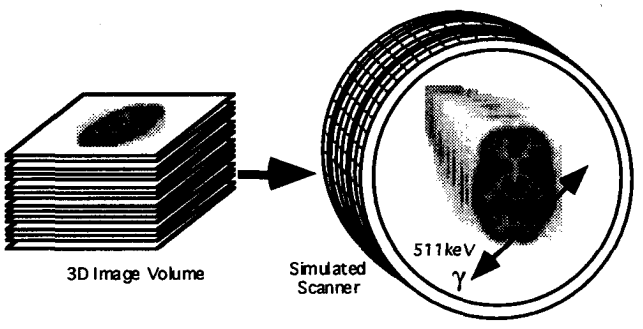

Fig. 1. Concept of using the stacked planes of the 3-D image volume as the input source distribution for a simulated 3-D PET acquisition to calculate the scatter distribution.

mary) and total (scattered + primary) photon pairs are calculated and sorted into their respective sinograms. The scatter component is equal to the difference between these two generated sinograms.

The flow chart for the simulation is shown in Figure 2. For this paper, three assumptions are made: (1) a photon is assumed to be detected where it strikes a detector surface (provided its energy is above a certain threshold), (2) the scatter from activity outside the field of view (FOV) is ignored (see Section IV), and (3) the linear attenuation coefficient for the head is uniform and equal to that of water (see Section IV). Multiple Compton scatters are allowed. The decision as to whether or not a given photon scatters is determined by both the linear attenuation coefficients of the medium and the distance from the photon's origin to the edge of the scattering medium along the line of propagation. For high statistics brain studies, the edge is currently determined by a threshold pixel value. For phantoms, the edge is defined

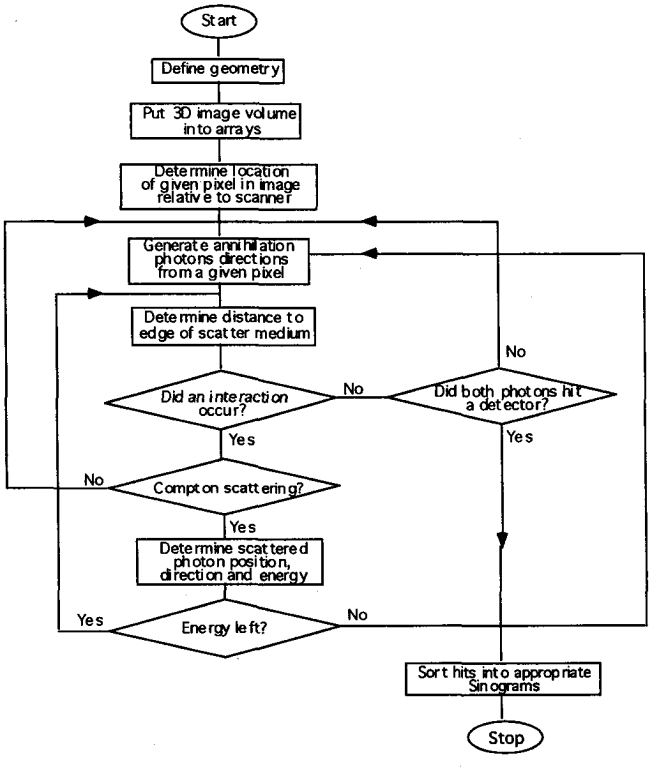

Fig. 2. Flow chart for the Monte Carlo calculation of Compton Scatter in 3-D PET.

by their known geometrical shape. The energy and direction of a scattered photon is determined by the Klein-Nishina cross-section formula. If the photon escapes the scattering medium and interacts with a detector in the gantry, the event is recorded in the appropriate sinogram as either a scatter or primary event depending on its energy. The energy threshold was set at 250 keV for these simulations.

III. RESULTS

A. Axial Opening Angle Dependence of the Scatter

The Monte Carlo scatter calculation was tested using 3-D acquired brain images from the CTI 831 NeuroECAT system with septa removed. The image volumes studied have 15 planes, each 128 x 128 pixels in size. Each pixel is 1.75 x 1.75 mm^2 and the axial separation between planes is 6.75 mm. Figure 3 (top) displays a schematic representation in coronal cross-section of two photons being emitted (a typical "scattered" event) in the scanner in a simulated 3-D PET acquisition; the axial opening angle α is defined as the angle that the direction of one of the emitted photons in a pair makes with the transverse plane; in general, α varies from 0 to 180°. However, in the simulation, there is a maximum range of α above which the calculated scatter fraction does not increase: the bottom portion of Figure 3 shows the manner in which the calculated scatter fraction varies with the maximum

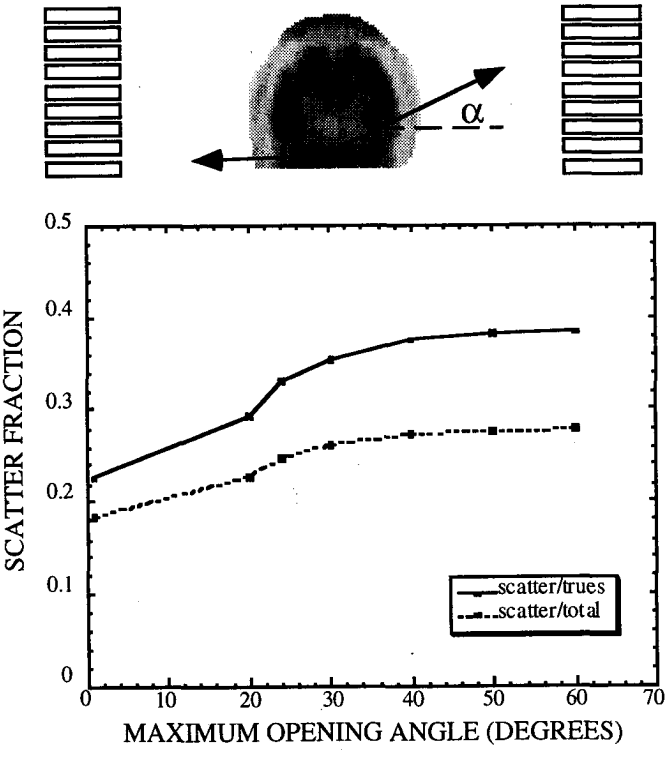

Fig. 3. Top: schematic representation of a coronal cross-section through the simulated 3-D PET scanner showing the opening angle α of one of the photons from a pixel in the input image volume. Bottom: calculated scatter fraction vs. maximum opening angle allowed for the first photon emitted in each event of a simulated 3-D human brain scan (trues = unscattered, total = trues + scattered).

axial opening angle allowed for of the first photon in every event the simulation. For an axial opening angle range greater than 40° the scatter fraction in a human brain saturates at roughly 38%. In order to reduce the fraction of undetected events, α was allowed to vary from 0 to a maximum value of 40° in further simulations.

B. Accuracy of the Modeling

Figure 4 shows a comparison between typical planes from the input image volumes of two 3-D acquired [2] and reconstructed [12] data sets (without scatter correction) and the corresponding Monte Carlo data generated from a simulated 3-D PET acquisition. A calculated attenuation correction was performed on the simulated primaries' sinograms [13] and the reconstruction was performed in 2-D using a ramp filter at the Nyquist frequency to retain the high frequency information. The simulated images correspond well with the input, indicating that the geometry and physics are adequately modeled: for example, when normalized to the same number of counts, the rms percent deviation about zero of the difference of the two images on the left of the upper row of Figure 4 was about 9% (Fig. 4c, top), with the maximum deviation at the skull. Within the skull, the corresponding rms deviation value was roughly 5%. The large discrepancy at the skull and scalp is largely due to the approximation of a constant linear attenuation coefficient for the head. The fractional difference images in Figure 4c are consistent with the fact that inside the skull, the largest error in our normalized comparison between images will occur where the activity is lower: a noise pattern is seen corresponding to the lower count white matter structures.

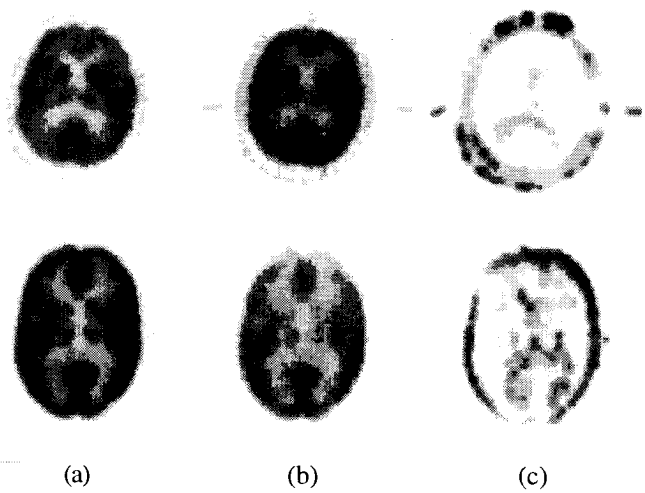

Fig. 4. A comparison between the 3-D image volume input (a) and the reconstructed emission data generated by the simulation (b) for a human brain (upper row) and the Hoffman brain phantom (lower row). Note the simulated data have less events than the input images. (c) the fractional difference between (a) and (b) when the two are normalized to the same total number of counts. The images are scaled to have the image maximum as the darkest pixel.

C. Subtraction of the Scatter Component

Because of the lower number of events in the Monte Carlo generated data sets as compared to the input (see Fig. 4), it was necessary to scale the simulation to match the measured data sets. The scale factor was derived from the scatter plus true simulated data and the uncorrected data from the scanner. The scatter correction is obtained by subtracting the scaled and smoothed scatter calculation from the original data set with normalization. After scatter subtraction, the 3-D data set is corrected for attenuation and then reconstructed using a version of the PROMIS algorithm [12]. Figure 5a displays four image planes from the uncorrected and scatter corrected 3-D Hoffman Brain Phantom. The corrected images have poorer signal-to-noise ratio but better overall contrast than the uncorrected original images. Figure 5b shows profiles through a sinogram of the original emission data without and with the Monte Carlo calculated corrections. Note how the scatter-corrected profile drops to zero at the edge of the phantom.

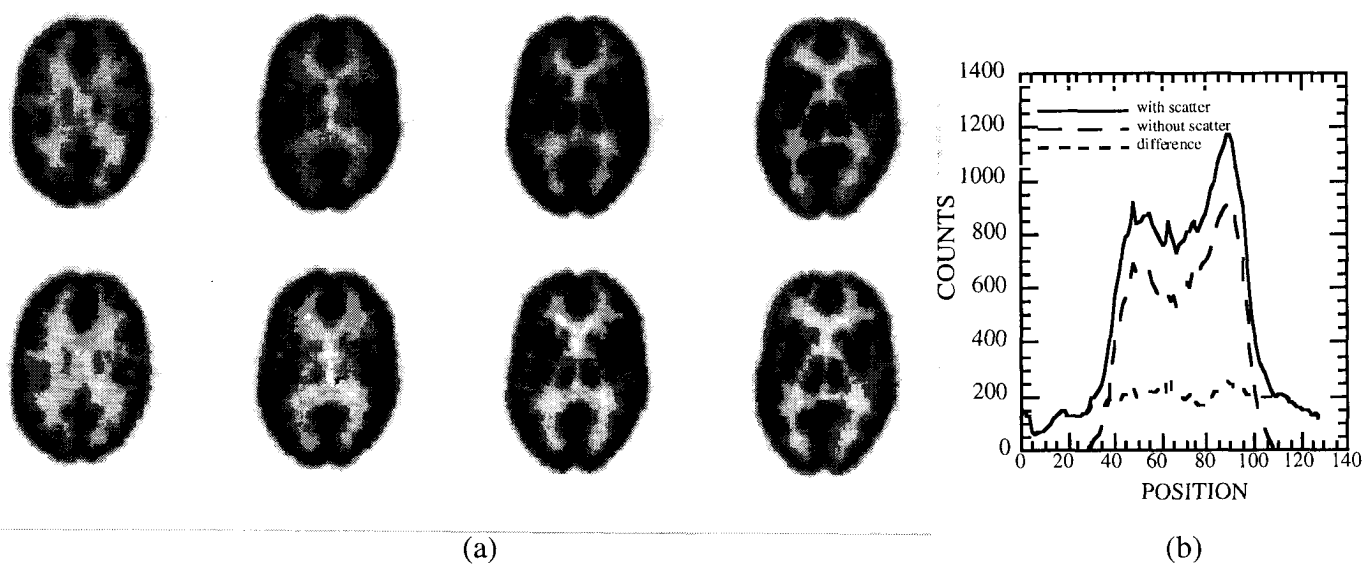

Fig. 5. (a) top row: uncorrected 3-D image volume (Hoffman Brain Phantom); bottom row: with Monte Carlo scatter correction. (b) a profile through one angle of the 3-D uncorrected and Monte Carlo corrected sinograms of the second plane shown in (a); there were no significant negative values.

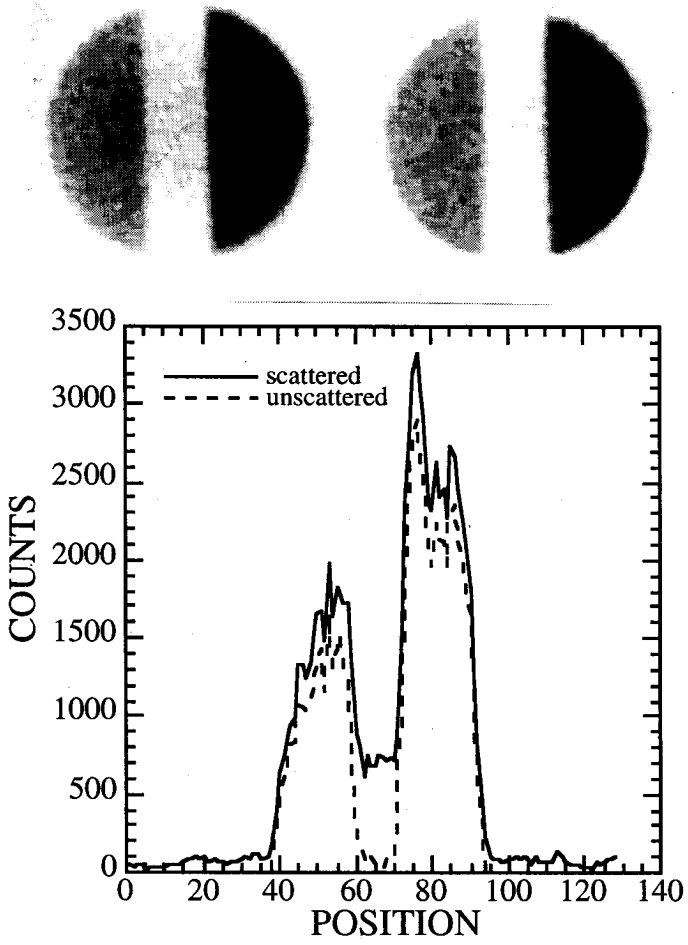

Fig. 6. Above: one plane from the uncorrected (left) and scatter-corrected (right) 3-D Slot Phantom image volume; and below: profile through one angle of the corresponding sinogram.

A more quantitative measure of the accuracy of the scatter correction can be obtained from Figure 6, which shows the results of the scatter correction for a 3-D slot phantom. In this figure the 3-D reconstructed images and smoothed profiles through a typical sinogram (attenuation corrected) are shown. Within the slot the only activity that is seen is due to scatter. The Monte Carlo calculated correction successfully brings the activity to zero outside the object. Since the input image volume already contained scatter, the calculation will over estimate the scatter; scatter subtraction within the slot thus resulted in some negative values. Using the left half of the corrected image (Fig. 6 top, right) as the reference "trues", the scatter/true fraction within the slot of the uncorrected image (Fig. 6 top, left) was approximately 40%, while the integrated activity/trues in the slot of the corrected image was roughly -2% (< -1% of total image). The statistical fluctuations within the slot are greater than the systematic negative errors introduced by including scatter in the input.

D. The Computation Time

The input image volumes discussed above were sampled pixel by pixel in the Monte Carlo simulation. Using this fine sampling the total execution time of the program was, for most cases, approximately 25 CPU hours using a Sun Sparc Station10. If we assume that the Compton scatter distribution is slowly varying over the object, coarser sampling of the input image volume is justified. By sampling over regions equivalent to 4x4 pixels, the execution time of the calculation was reduced by over an order of magnitude to less than 2 hours. Figure 7 shows smoothed profiles through attenuation corrected scatter sinograms simulated with both fine and coarsely sampled input. The two calculated scatter distributions compare well (overall to within 6% in mean number of counts) indicating that little error in the calculation of the scatter contribution is introduced by coarser sampling. For the finely-sampled simulation, scattered events comprise approximately 38% of the primary photon pairs detected.

Since one of the goals in this work is to preserve the accuracy of the scatter calculation, the finest sampling consistent with acceptable execution times will be used in practice. The more coarse the sampling of the input image data, the worse the blurring will be in the simulated emission data sets of scattered and unscattered photons, and the more inaccurate the scatter estimation. It should be noted that the current software is research grade code that requires optimization. We have assembled a workstation configured as eight i860 array processors [14] that we expect will improve the computation time by over a factor of 20 relative to a single Sparc10 CPU. Preliminary tests show that a single i860 chip was over 3 times faster than a Sparc10 CPU for calculations similar to those involved in the Monte Carlo code. With eight of such processors running in parallel, the expected computation time of the simulation for the fine (coarse) sampling case would be < 1 hour (5 minutes).

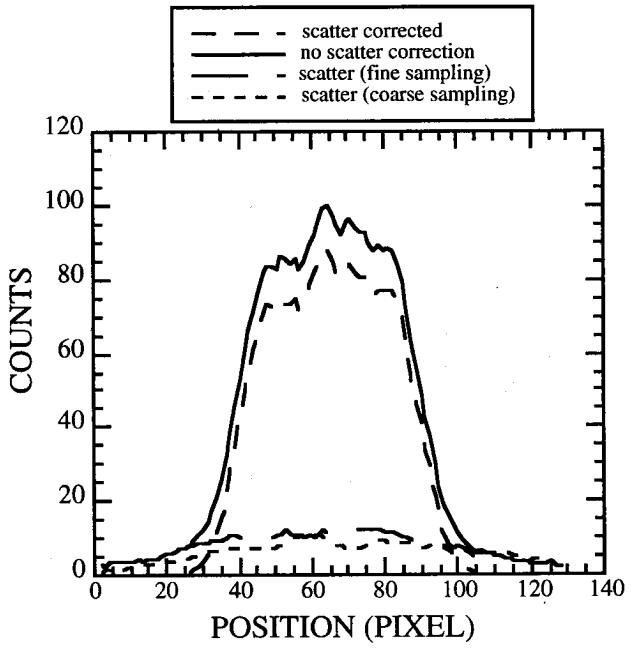

Fig. 7. Profiles through the sinograms of the Monte Carlo calculated uncorrected, corrected and scatter distributions for a 3-D human brain study (Legend shown at top); there were no significant negative values. The calculated scatter distributions for the coarse and finely sampled cases compare well. Computation time for coarse sampling is nearly a factor of 16 times shorter than for fine sampling.

IV. DISCUSSION

The motivation for developing this Monte Carlo correction for Compton scatter in 3-D PET is twofold: 1) For 2-D PET, one had a situation in which scatter was a 10-20% effect added to a technique that realistically expects no better than 10% accuracy. In that case, a 30% error in the scatter estimate would cause only a 3 to 6% error in the result. For 3-D PET, the scatter component is 40 to 60 % of the trues, and errors in the scatter estimate become large compared to other systematic errors; a higher degree of accuracy in the scatter correction is, thus, required. 2) For 3-D whole body PET, an accurate and efficient scatter correction is desirable to avoid diagnostic errors in whole-body surveys for tumor metastases. The generally poor statistics and large imaging area required puts strict limitations on the types of scatter corrections that are appropriate. Because the data sets are large and of low resolution, the scatter correction method must be fast but not necessarily of high resolution. We have thus emphasized the use of coarse sampling.

Our preliminary results indicate that the Monte Carlo approach to scatter correction of fully 3-D PET brain images is highly accurate with execution times that are close to being in an acceptable range for clinical use. In general, the technique requires no assumptions of the shapes of the source or scatter distributions or the physics of Compton scattering. No computational approximating techniques have yet been utilized. The scatter component of the total activity was calculated for complex activity distributions represented by the reconstructed 3-D image volume.

Images containing scatter are used as an initial estimate of the isotope distribution. This assumption results in an over-estimation of the scatter. In general, the extent of the overestimation depends on the physical situation. Activity in the empty compartment of a slot phantom was reduced to (i.e. over corrected by) approximately -5% of its value before correction, which corresponds to less than -1% of the entire corrected data set. If desired, the correction could be applied iteratively to reduce the error introduced by scatter in the input.

There is compelling evidence that ignoring scatter from data outside the FOV is not a valid assumption. It was utilized in this paper only as a matter of convenience (only one PET scan was required). In reality this contribution could be accounted for with a second scan after shifting the patient or phantom upward in the scanner. A proper superposition of this second data set onto that measured from the first scan would then be used as input to the Monte Carlo. It should also be realized that the entire motivation for this study was to develop an accurate scatter correction technique for 3-D whole body PET imaging. In that case, data measured from the entire body is included as input to the Monte Carlo.

The other major assumption apparent in the calculation is the assumption of a constant attenuation coefficient, ignoring bone and air spaces. These details are usually neglected in calculated attenuation corrections which produces errors similar to those found in measured attenuation correction (a trade-off between error due to scatter in the measured technique and error due to the assumption of constant attenuation coefficient in the calculated correction). In the full development of this Monte Carlo technique for scatter correction, it will be necessary to better characterize the attenuation coefficient for the lungs in the thorax and additional phantom studies will be required to estimate the error due to assumptions used in this method.

Our computing system to be used for the calculation, with two quad i860 boards, is compatible with current commercial hardware: the major manufacturers of PET systems (GE Medical Systems, Milwaukee WI and Siemens/CTI PET Systems, Knoxville, TN) have current scanners available with quad i860's.

V. ACKNOWLEDGMENTS

The authors thank S Cherry, S Siegel and P Banerjee for suggestions and technical guidance. This research was funded by NIH Grants T32 CA09092 and R01-CA56655, DOE Grant DE-FC03-87-ER 60615 and the Whitaker Foundation.

VI. REFERENCES

[1] ME Phelps *et al:* An Analysis of Signal Amplification Using Small Detectors in Positron Emission Tomography. *J Comp Assist Tomogr* 6:551 (1982).

[2] SR Cherry, M. Dahlbom and E.J. Hoffman. 3-D PET Using a Conventional Multi-slice Tomograph without Septa. *J Comput Assist Tomogr* 15(4):655 (1991).

[3] DW Townsend *et al:* Fully 3-Dimensional Reconstruction for a PET Camera with Retractable Septa. *IEEE Trans Med Im* 10(4): 505 (1991).

[4] S Grootoonk,*et al:* Correction for Scatter Using a Dual Energy Window Technique with a Tomograph Operating without Septa. *IEEE Med Im Conf Rec*, 3:1569 (1991).

[5] DL Bailey: 3-dimensional Acquisition and Reconstruction in Positron Emission Tomography *Ann Nucl Med* 6:123 (1992).

[6] L Shao and JS Karp: Cross-Plane Scatter Correction-Point Source De-convolution in PET. *IEEE Trans Med Im* 10(3):234 (1991).

[7] SR Cherry, SR Meikle and EJ Hoffman: Correction and Characterization of Scattered Events in Three Dimensional PET Using Scanners with Retractable Septa. *J Nuc Med* 34:671 (1993).

[8] SR Cherry and SC Huang: Correction and Characterization of Scatter in 3-D PET. *Presented at the 1994 IEEE Medical Imaging Conference.*

[9] JM Ollinger and GC Johns: Model-based Scatter Correction for Fully-3-D PET. *Conf Rec 1993 Meeting on Fully 3-dimensional Image Reconstruction*, p. 111.

[10] JS Barney, R Harrop and CJ Dykstra: Source Distribution Dependent Scatter Correction for PVI. *IEEE Trans Nucl.Sci* NS-38:719 (1993).

[11] M Dahlbom *et al*: A Study of the Possibility of Using Multi-Slice PET Systems for 3-D Imaging. *IEEE Trans Nuc Sci* NS-36:1066 (1989).

[12] SR Cherry, M. Dahlbom and E.J. Hoffman: Evaluation of a 3-D Reconstruction Algorithm for Multi-slice PET Scanners. *Phys Med Biol* 37(3): 779 (1992).

[13] S Siegel and M Dahlbom: Implementation and Evaluation of a Calculated Attenuation Correction for PET. *IEEE Trans Nuc Sci* NS-39:1117 (1992).

[14] TM Guerrero *et al*: 3-D PET Reconstruction Workstation: 1. Design and Construction. *IEEE Conf Rec*, 2: 1096 (1993).